Journal of Molecular Structure 1262 (2022) 133057

Contents lists available at ScienceDirect

Journal of Molecular Structure

journal homepage: www.elsevier.com/locate/molstr

Electrolyte effect on the electroactuation behavior of multilayer polypyrrole films intercalated with $TFSi^-$, ClO_4^-, NO_3^- anions in lithium and potassium based electrolyte solutions

Zoltán Novák, Gábor Kozma, Ákos Kukovecz*

Interdisciplinary Center of Excellence, Department of Applied and Environmental Chemistry, University of Szeged, Rerrich Béla tér 1., H-6720, Hungary

ARTICLE INFO

Article history:
Received 30 January 2022
Revised 5 April 2022
Accepted 9 April 2022
Available online 14 April 2022

Keywords:
Polypyrrole
Electroactive polymers
Electroactuation
Artificial muscle
Potassium
Electrolyte
Arduino

ABSTRACT

We report on a comparative study on the electroactuation behavior of polypyrrole films doped with K^+ and Li^+ based electrolytes containing $TFSi^-$, ClO_4^-, or NO_3^- anions. Multilayer polypyrrole-gold-polyvinylidene fluoride (PPy-Au-PVDF-Au-PPy) films were fabricated via electrooxidative pyrrole polymerization in a solution containing various lithium (LiTFSi, $LiClO_4$, $LiNO_3$) and potassium (KTFSi, $KClO_4$, KNO_3) electrolytes. The electroactuator behavior was tested in different media (air, Adriatic seawater, native electrolyte solutions, and Dulbecco's phosphate buffer saline solution). PPy films intercalated with KTFSi exhibited particulary good performance in air, remaining electroactive for over 40 days and withstanding over 230 actuation cycles while maintaining at least 50% of their original displacement capacity.

1. Introduction

Electroactive polymers (EAPs) are desirable candidates for applications including actuators functioning in air and vacuum [1,2], miniature wearable devices [3,4], tactile displays and drug delivery systems in healthcare and biomedicine [5–7], electric power generation and storage [8,9], signal sensing and processing [10,11], electrocatalysts and biosensors [12,13] and anticorrosive coatings and electromagnetic shields [14,15]. A recently developed, hydraulically amplified, self-healing electrostatic (Peano-HASEL) actuator [16] re-evaluated the importance of EAPs as artificial muscles in healthcare and robotic systems. EAPs are able to produce mechanical strain through redox reactions inside the substrate when under electrode potential control, resulting in motion by converting input electrical energy into mechanical energy.

Electroactive polymers are either dielectric elastomers (DEAPs) or ionic electroactive polymers (IEAPs). Though both are lightweight and have a relatively high elastic energy density, the former requires high activation voltage (in the range of kVs) to produce large actuation strain rates (even up to 300% [17]), while the latter is capable of bending by changing its volume due to the movements of charged particles (cations and anions) in the substrate containing the electrolyte solution. Ion transport in IEAPs is controlled by the applied voltage and its orientation depends on the voltage polarity. The electromechanical response strongly corresponds to the nature of the constituent electrolyte (specifically, the solvated radius and mobility of its cations) and its integration into the insulating and porous substrate [18]. The constituent ions are typically inserted into the substrate from the electrolyte solution by doping. Doping is achieved by the electrochemical oxidation (p-doping) or reduction (n-doping) of a polymer. Charged species formed upon this process are able to move along the carbon chain of the polymer allowing electron transport, hence evolving into an electronically conductive material. When electrical voltage is applied, electrons are extracted (oxidation) or inserted (reduction) along the polymer backbone causing ion movements to ensure complete electroneutrality in the system.

Polypyrrole (PPy), a polymer based on a heterocyclic aromatic compound, is of particular interest due to its high electrical conductivity, interesting redox properties and the simplicity of its synthesis [19]. It is among the most promising candidates to develop electrochemical biosensors, conductive textiles, mechanical actuators and anti-corrosion coatings. The synthesis of PPy can be either chemical or electrochemical, the latter being the more efficient and balanced one [20,21]. Electro oxidative polymerization or elec-

* Corresponding author.
E-mail address: kakos@chem.u-szeged.hu (Á. Kukovecz).

https://doi.org/10.1016/j.molstruc.2022.133057
0022-2860/

trodeposition is usually executed in a three electrode cell containing (i) a working electrode, where the chemistry of interest occurs (electrodeposition in our case); (ii) a counter electrode allowing charge to flow through the cell, while maintaining balanced current on the working electrode; and (iii) a reference electrode acting as a reference in measuring and controlling the working electrode potential without passing any notable amount of current. The conductive polymer film grows at the substrate/monomer double layer by the anodic oxidation of the monomer from the electrolyte solution due to the processes at the substrate/monomer double layer [21,22]. In these solutions the charged particles (cations: K^+, Li^+; anions: $TFSi^-$, ClO_4^-, NO_3^-) migrate toward the oppositely charged terminals of the cell. Anions are inserted into the substrate (doping), while the cations enhance the solution properties to improve the effectiveness of the polymerization process. Dopants and counter anions play an important role in the physicochemical properties, morphology and the conductivity of an EAP material [23].

A stable functional electrolyte solution is a key component in almost all electrochemical devices such as fuel cells, capacitors, batteries and multielectrode electrochemical cells [24–26]. Electrolytes consist of ionic salts dissolved in a polar solvent such as water, acetonitrile or propylene carbonate. The nature of the charged particles (anions, cations) and their ionic conductivity and mobility determine the efficacy of such electronic devices. The choice of the electrolyte and the solvent is crucial from the EAP point of view, because the ionic conductivity influences the redox process as a whole during electropolymerization and also in electromechanical actuation. The efficiency of electropolymerization depends on several factors such as the applied current density, the composition of solution, electrolyte concentration, morphology and roughness of the substrate electrode, and other environmental factors [20–22,27]. A change in any of the these parameters could affect the conductivity, hence the electromechanical behavior of the resulting PPy films.

K. Kubota et al. have recently discussed the advantages of alternative alkaline fuel cells, batteries and electrolyzers [28]. The number of studies on high-performance potassium batteries and the effectiveness of potassium in the ion migration process is constantly increasing [29–33]. Here, we take this approach a step further to explore whether potassium electrolytes could serve as an alternative to the lithium-based ionic liquids used in IEAP actuators [34–37]. Commercial and industrial use of IEAPs need to be optimized in repeatability, energy density and durability [37]. In this study we report on the electromechanical effect of different lithium and potassium ionic liquids on PPy films. Our results suggest that K-electrolytes can outperform Li-electrolytes in the terms of IEAP operation.

2. Experimental

2.1. Formulae, definitions and units

1. *Positive/negative half-cycle:* bending of the samples from the initial position (open circuit) to maximum displacement (a positive or a negative elongation) then back to its initial position.
2. *Half cycle duration (t_{hc}):* the duration of a half cycle.
3. *Peak half cycle duration ($t_{hc,p}$):* the minimum half-cycle duration of a PPy film.
4. *Peak voltage (V_p):* the applied voltage at the lowest half-cycle duration (fastest bending).
5. *Total number of actuation cycles (N_C):* one actuation cycle equals two consecutive half cycles (one positive and one negative elongation).
6. *Days of electroactivity (D_E):* the active days for which the films actuated.

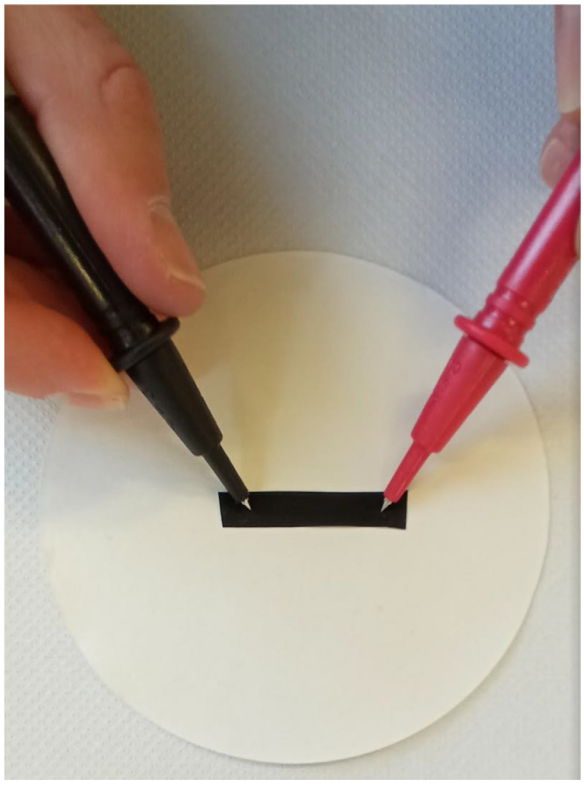

Fig. 1. Resistance measurement of a PVDF-Au-PPy sample with a digital multimeter.

2.2. Preparation of the working electrodes

PVDF membranes (Durapore Membrane Filter, 0.22 µm/140 mm, hydrophilic) were cut into equal rectangles (1.5 × 7 cm^2) and gold plated on both sides by magnetron sputtering applying a sputter current of 22 mA for 12 min in a sputter vacuum of $7{\cdot}10^{-2}$ mbar (Quorum Tech Q150R S, Rotary Pumped Coater). The apparatus is illustrated schematically in the left panel of Fig. 2.

The electrical resistance of the resulting conducting gilded films was 8–13 Ω as measured with an ANENG DT9205A digital multimeter (Fig. 1). These resistances were measured longitudinally between both ends of our samples. We paid attention to putting the probes of the multimeter 0.5 cm from the ends, when determining the resistance.

2.3. Preparation of the electrolyte solutions

Six different electrolyte solutions were tested. They were all based on acetonitrile solutions (AN, anhydrous, ≥99.5%, VWR Chemicals) containing 2 wt% methanol (anhydrous, 99.8%, Sigma Aldrich). The salts were freeze dried at 0.25 mBar and −52 °C (LABCONCO Freeze Dryer) for 72 h, then dissolved in the AN to achieve 0.05 M concentration of bis(trifluoromethanesulfonyl)imide potassium (KTFSi, Reagent Plus 97%, Sigma-Aldrich), bis(trifluoromethanesulfonyl)imide lithium (LiTFSi, 99%, ACROS Organics), potassium perchlorate ($KClO_4$, 99%, ACS Reagent), lithium perchlorate ($LiClO_4$, ACS Reagent ≥95%, Sigma-Aldrich), lithium nitrate ($LiNO_3$, Sigma-Aldrich), and potassium nitrate (KNO_3, 99%, Molar Chemicals). Freshly distilled pyrrole (Py, extra pure, 99%, Acros Organics) was added to the solutions in 0.2 M concentration without further cleaning under magnetic stirring. The electrolytes were stored at 4 °C until use. Dulbecco's phosphate buffer saline solutions (DPBS) with 1 M of DPBS (dry powder modified without calcium and magnesium,

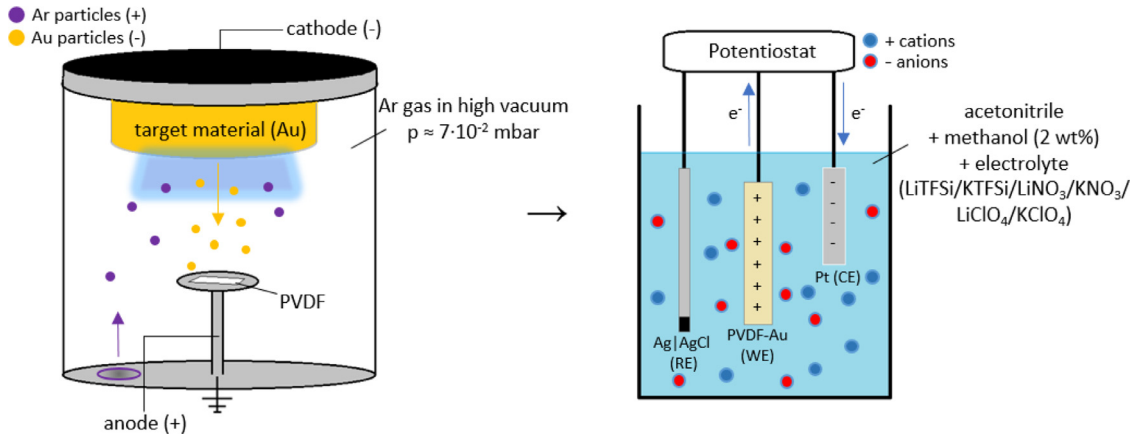

Fig. 2. Schematic illustration of the sputter coating of PVDF substrates and the galvanostatic electrodeposition of pyrrole.

Sigma Aldrich) were also prepared for testing the actuation behavior of the PPy films.

2.4. Chronopotentiometric synthesis of polypyrrole

The electrodeposition of polypyrrole films was performed in a three-electrode electrochemical cell using a Metrohm Autolab PGSTAT302N potentiostat. A counter electrode (Pt sheet electrode, 3.5 × 1.5 cm), a reference electrode (Ag/AgCl solid state electrode) and a working electrode (gilded PVDF membrane) were immersed into the electrolyte, then a constant current of 4 mA was applied for 1 h for each sample. The setup is illustrated in the right panel of Fig. 2. The offset time was set to 60 s. The process was carried out at -16 °C. The temperature was maintained by a cooling bath in a thermostat containing acetone (Technical ≥99%, VWR Chemicals), ice cubes and sodium chloride. All the potentials are given here relative to the Ag/AgCl reference electrode. The characteristic chronopotentiograms measured for each electrolyte are depicted in Fig. 3.

2.5. Characterization of PPy films

The freshly synthesized PPy films were characterized by scanning electron microscopy (Thermo Scientific Apreo 2, field emission SEM). Scanning electron microscopic images were captured using 10 kV accelerating voltage with various magnifications (1 000× and 10 000×). The structure of the differently doped PPy films was studied by Raman spectroscopy (Senterra II Raman microscope). All Raman spectra were measured with a resolution of 4 cm^{-1} at 532 nm with 6.25 mW laser power (30 s accumulation time, 16 number of exposures).

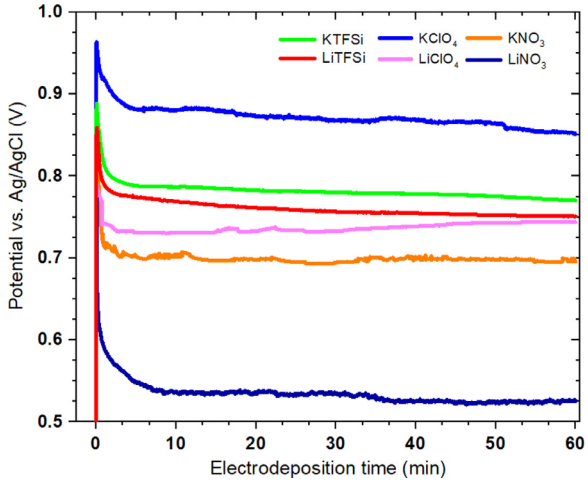

Fig. 3. Chronopotentiograms in different electrolyte solutions (AUTOLAB Metrohm) during galvanostatic electrodeposition of pyrrole.

2.6. Electroactuation and tip displacement measurements

The edges of the PPy films were cut off to prevent shorting between the conducting layers. Samples were stored at 4 °C in their respective electrolyte solutions. Electroactuation experiments were conducted in four different media: air, adriatic seawater, electrolyte storage solutions and DPBS solution with the help of an Arduino UNO module linked to an L298N DC Motor Driver. Samples were kept at room temperature for 30 min before measurement. All measurements were carried out at room temperature (25 °C). Samples were fixed at one end with an insulating clip and allowed to bend when exposed to voltage delivered through insulated wire contacts. Further information about the Arduino microcontroller schematic and photographic documentation of the measurement configuration are available in the Supporting Information.

For the tip displacement measurements of our films, we used a millimeter paper and a camera in order to differentiate the effects of the used electrolytes (Fig. 4). Each of the samples was soaked in their corresponding storage solution and had been taken out from the fridge (0–4 °C), before measurements. One of the ends of our PPy films were fixed and the maximum elongation of our samples were recorded until the bending was completely stopped.

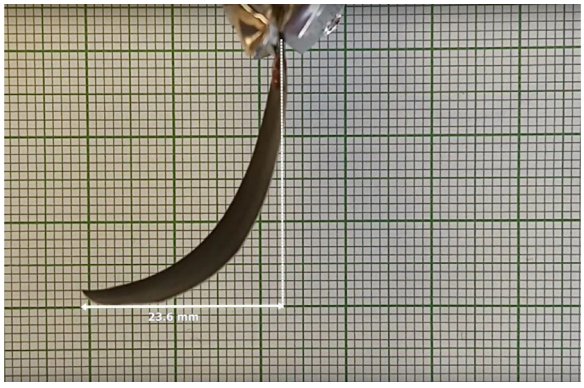

Fig. 4. Displacement measurements were carried out over a millimeter paper for the differently doped PPy films, while the corresponding average peak voltage was applied.

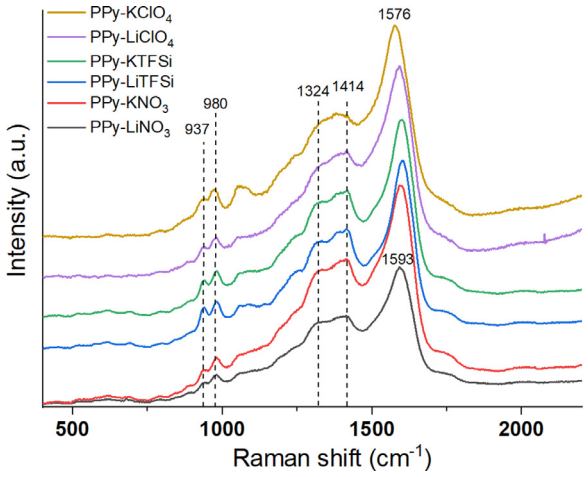

Fig. 5. Raman spectra of PPy films synthesized in different electrolyte solutions.

3. Results

3.1. Characterization

The well-known cauliflower-like SEM patterns of PPy were identified in the SEM images (Supporting information, Figures S1-S3) [38]. The surface of PPy-TFSi$^-$ samples was more homogeneous than those of PPy-ClO_4 and PPy-NO_3 films.

Fig. 5 presents the Raman spectra of the electrodeposited PPy films. All characteristic polypyrrole peaks are clearly observable [39]. The highest intensity peak at 1593 cm^{-1} is assigned to the C=C double-bond of the PPy in the oxidized form. The peaks near 1414 and 1324 cm^{-1} correspond to C–N stretching, whereas those near 980 and 937 cm^{-1} are associated with the C–H stretching vibrations. The C=C double bond in the Raman spectra slightly differs for each sample as it shifts towards lower wavenumbers at more negative applied potentials during the electrosynthesis [39].

3.2. Preliminary analysis

Preliminary analysis was performed to measure the electrical resistance, the voltage range of operation, and the half cycle duration (t_{hc}) of the films (Fig. 6). We applied voltages from −5 V to +5 V with a voltage step of 0.1 V to each type of film in the presented media and analysed their actuation. The chronopotentiograms (Fig. 3) are symmetrical to the minimum value of the half-cycle duration called peak half-cycle duration ($t_{hc,p}$), hence indicating the fastest actuation at the corresponding peak voltage (V_p) (Table 1). Electroactuation happened at both positive and negative voltages, it was only the direction of the curvature that was reversed upon polarity change. All curves exhibited a discontinuity at low absolute voltages where no actuation occurred and only oc-

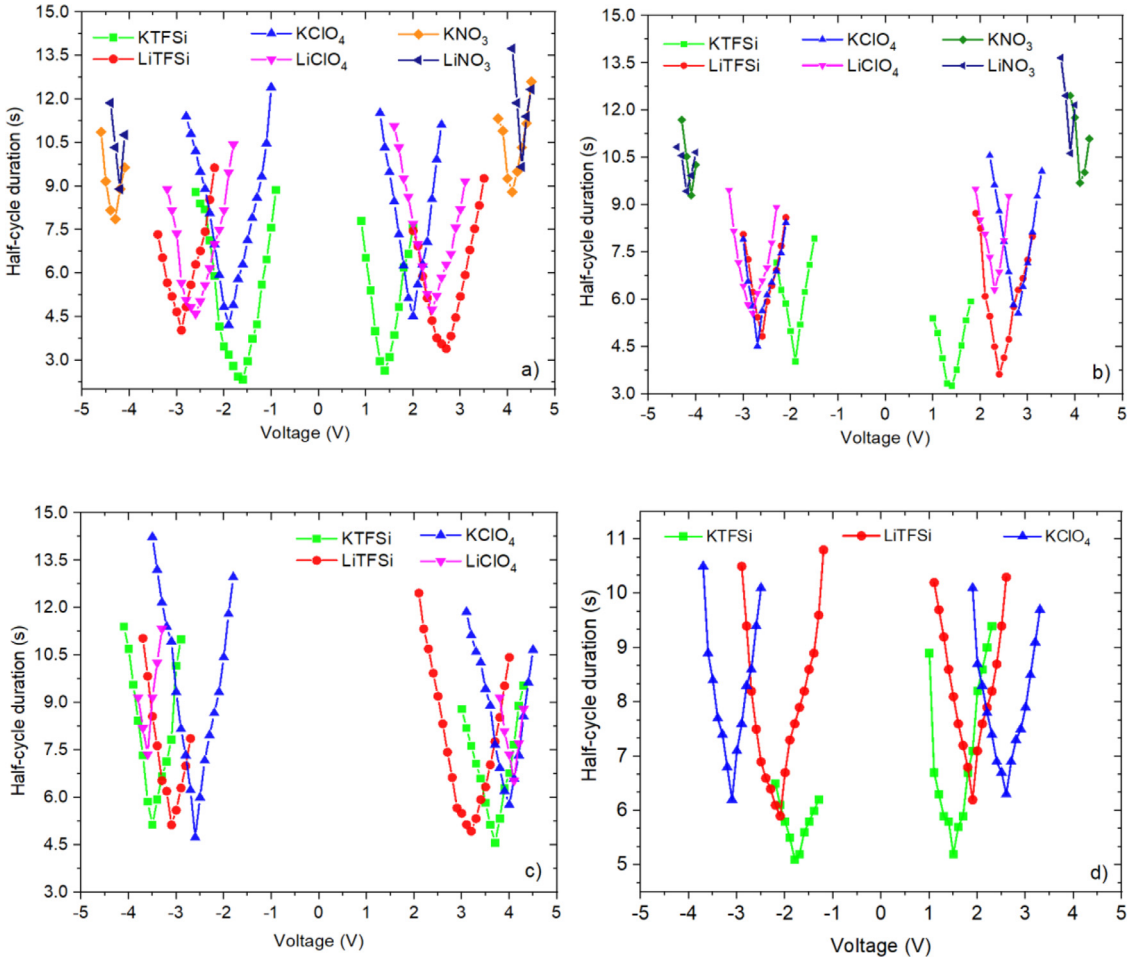

Fig. 6. The mean half cycle durations over the applied voltage of the PPy samples. Voltage was applied between −5 V to +5 V with a step rate of 0.1 V in order to determine the voltage range and the peak voltage (V_p) at which the half-cycle duration ($t_{hc,p}$) is the lowest. Measurements were conducted in air (a), electrolyte solutions (b), adriatic seawater (c) and 1 M DPBS solution (d); x-axis is the applied voltage (V), y-axis shows half-cycle duration (t_{hc}).

Table 1
Peak voltages ($\pm V_p$) and peak half cycle durations ($t_{hc,p}$) of the our doped PPy films in air, adriatic seawater, different electrolyte solutions and 1 M DPBS solution at negative and positive cycles. Standard deviations (Eq.S1) were calculated from the dataset of three samples for each type of constituent.

Ionic salt	Air				Adriatic sea water			
	V_p (V)		$t_{hc,p}$ (s)		V_p (V)		$t_{hc,p}$ (s)	
	−	+	−	+	−	+	−	+
KTFSi	1.6 ± 0.3	1.4 ± 0.4	2.3 ± 0.4	2.6 ± 0.3	3.5 ± 0.3	3.7 ± 0.2	5.1 ± 0.5	4.6 ± 0.7
LiTFSi	2.9 ± 0.4	2.7 ± 0.3	4.0 ± 0.5	3.4 ± 0.4	3.1 ± 0.3	3.2 ± 0.2	5.1 ± 0.3	4.9 ± 0.6
$KClO_4$	1.9 ± 0.3	2.0 ± 0.2	4.2 ± 0.3	4.5 ± 0.2	2.6 ± 0.2	4.0 ± 0.4	4.7 ± 0.4	5.6 ± 0.5
$LiClO_4$	2.6 ± 0.3	2.4 ± 0.4	4.6 ± 0.7	4.7 ± 0.6	3.6 ± 0.4	4.1 ± 0.3	7.4 ± 0.6	6.5 ± 0.3
KNO_3	4.3 ± 0.2	4.1 ± 0.5	7.9 ± 1.2	8.8 ± 1.4	–	–	–	–
$LiNO_3$	4.2 ± 0.4	4.3 ± 0.7	8.9 ± 0.8	9.7 ± 0.9	–	–	–	–
Ionic salt	Electrolyte solution				1 M DPBS			
	V_p (V)		$t_{hc,p}$ (s)		V_p (V)		$t_{hc,p}$ (s)	
	−	+	−	+	−	+	−	+
KTFSi	1.9 ± 0.2	1.4 ± 0.3	4.0 ± 0.4	3.3 ± 0.3	1.8 ± 0.2	1.5 ± 0.1	5.1 ± 0.4	5.2 ± 0.7
LiTFSi	2.6 ± 0.3	2.4 ± 0.5	4.8 ± 0.6	3.6 ± 0.5	2.1 ± 0.1	1.9 ± 0.4	5.9 ± 0.5	6.2 ± 0.8
$KClO_4$	2.7 ± 0.1	2.8 ± 0.2	4.5 ± 1.2	5.6 ± 0.9	3.1 ± 0.3	2.6 ± 0.5	6.2 ± 0.8	6.3 ± 0.4
$LiClO_4$	2.8 ± 0.4	2.3 ± 0.4	5.6 ± 0.8	6.3 ± 1.1	–	–	–	–
KNO_3	4.1 ± 0.3	4.1 ± 0.5	9.3 ± 1.3	9.7 ± 0.6	–	–	–	–
$LiNO_3$	4.2 ± 0.1	3.9 ± 0.3	9.4 ± 0.6	10.6 ± 1.2	–	–	–	–

Table 2
The number of actuation cycles (N_C) in different media. Standard deviations (Eq.S1) were calculated from the dataset of three samples for each type of constituent. Lack of data indicates that the film did no actuate in that particular media at all.

Ionic salt	Number of actuation cycles (N_C)			
	Air	Adriatic sea water	Electrolyte solution	1 M DPBS solution
KTFSi	235±6	69±4	145±7	71±4
LiTFSi	185±8	54±3	121±4	77±6
$KClO_4$	124±5	60±2	63±2	41±5
$LiClO_4$	73±3	43±6	82±6	–
KNO_3	31±4	–	19±2	–
$LiNO_3$	39±2	–	3 ± 3	–

cassional small random movements were detected. Depending on the ionic salt in the electrolyte solution, high voltages (higher than +5 V or lower than -5 V) applied for more than half a minute tend to burn through and ruin the PPy films. The PPy-KTFSi films were actuated with a significantly lower peak voltage and peak half-cycle duration regardless of the media they were tested than any other of our samples. In the case of PPy-KNO_3 and PPy-$LiNO_3$, in seawater and 1 M DPBS solution, and in the case of $LiClO_4$ in 1 M DPBS solution, actuation was not observed at all (Table 1).

3.3. Electroactuation behavior

The determined peak voltages (reported in Table 1) were applied to the films in an infinite loop. The number of acutation cycles (N_c) was defined as the point where the electroactuated displacement of the film dropped below 50% of its initial value. N_c values are reported in Table 2 as averages of measurings three independent samples. The PPy-KTFSi films were superior in almost all of the media, but especially in air. In seawater the films degraded more quickly.

Durability measurements were conducted to reveal how the films can withstand the passage of time in the aforementioned media. The films were subjected to their respective determined peak voltages (V_p) once every day until their electoactuated displacement dropped below 50% of its initial value. This point of defined as the number of electroactive days (D_E). When not under testing, the PPy films were stored in their corresponding electrolyte solutions. Table 3 reports the D_E values for each sample as averages of three independent sample measurements.

Potassium electrolytes, especially KTFSi and $KClO_4$ were found to be substantially more durable compared to the other samples. According to the data represented in Table 3, KTFSi samples were approx. 30% more active than LiTFSi samples.

4. Discussion

For the fabrication of PPy conductive films, we used a galvanostatic electro oxidative polymerization method in which we made sure to put the electrodes as close to each other as possible in order to minimize the ohmic drop (ΔU_Ω = - I_cR, where I_c is the flowing current and R is the solution resistance). During the electropolymerization, active particles (radical cations) are generated due to the oxidation of the conjugated monomer on the electrode substrate by passing electric current throughout the cell. An offset time of 60 s, which is the duration we waited after assembling the cell, was set as a fail safe switch before starting the electropolymerization process in the potentiostat's software. In addition, this also can be also considered as a „relaxation time" for the following. As the amount of redox charges, thus the quality of PPy layers on the electrode highly depends on the movement of the electrolyte solution surrounding the electrodes [21], to provide efficient PPy films with high conductivity, preventing the movement of the solution in

Table 3
The days of electroactivity (D_E) in different media. Standard deviations (Eq.S1) were calculated from the dataset of three samples for each type of constituent. Lack of data indicates that the film did no actuate in that particular media at all.

Ionic salt	Electroactive days (D_E)			
	Air	Adriatic sea water	Electrolyte solution	1 M DPBS solution
KTFSi	42 ± 4	18 ± 3	46 ± 9	25 ± 2
LiTFSi	31 ± 3	23 ± 5	41 ± ±4	21 ± 4
$KClO_4$	27 ± 4	15 ± 2	21 ± 2	19 ± 3
$LiClO_4$	20 ± 5	11 ± 3	18 ± 5	–
KNO_3	6 ± 2	–	9 ± 4	–
$LiNO_3$	5 ± 1	–	7 ± 2	–

the macroscopic scale is advised before the electropolymerization started [20].

The polymerization was run below 4 °C at a constant temperature to produce conductive PPy films with a uniform structure [27]. The electrooxidation potential responses for the applied current were between 0.5 and 0.9 V in the chronopotentiograms (Fig. 3), which is the optimal potential window for PPy polymerization as the efficiency of the formation of the pyrrole monomer and the amount of redox charges are the highest here [21].

The choice of a solvent was a critical success factor for the electrodeposition process because the physicochemical properties of the solution (nature of the solvent, viscosity, density, ionic conductivity and the constituent electrolyte) strongly affect the ion migration process during the deposition and the properties of the PPy films. Acetonitrile as an aprotic, polar solvent was an optimal choice due to its superior conductivity compared to other polar solvents [40]. Moreover, its aprotic nature minimizes nucleophilic reactions. Nucleophilic solvents must be avoided to support the continuous growth of PPy films, because nucleophilic solvent molecules do not interact with the radical cations during the monomer oxidation process [27].

The observed shift of the Raman peak corresponding to the C=C stretching vibration is related to the electrical conductivity of the differently doped, oxidized PPy layers. As the peak's wavenumber decreases, the electrical conductivity increases [39,41]. Thus, PPy-$KClO_4$ films have the highest (C=C bond at 1576 cm^{-1}), and PPy-LiTFSi (1601 cm^{-1}) and PPy-KTFSi (1597 cm^{-1}) films have the lowest electrical conductivity in the studied sample pool. Interestingly, according to the electroactivity measurements (Tables 1–3), the electroactuation behavior of the PPy films is governed by the nature of the electrolyte solution (ionic conductivity and viscosity) rather than the electrical conductivity of the films.

Ionic liquids as solvents used in an IPMC actuator have to have low viscosity, high conductivity and large anion and cation size difference to promote easier ion migration and larger actuation strain [42]. Ionic liquid properties depend on the present electrolyte. Although the properties of incorporated anions greatly affect the operation of ionic polymer films, the cations also affect the ion-solvent interactions, thus the ion migration in the solvent [43]. Amara et al. [43] stated that viscosity is a critical property considering the ionic mobility in an electrolyte solution, thus also the actuation of our PPy films. They also presented that Li^+ cations compared to K^+ cations could cause an elevated shear resistance toward the solution particles in acetonitrile, increasing the ion-solvent interactions during the migration process due to their larger solvated radius [43]. Therefore, K^+ cations make the solvent slightly less viscous than Li^+ cations due to their smaller solvated (Stokes) radius compared to Li^+. The lower viscosity in AN results in higher ionic mobility and conductivity than a Li^+-containing solution [44,45]. In case of our intercalated anions, we our PPy-$TFSI^-$ samples performed much better, than the ClO_4^- and NO_3^- containing films due to the larger ionic radius of the $TFSi^-$ anion (329 pm) due to the aforementioned larger anion and cation size difference [42,46].

The obtained electroactuation behavior data (Tables 1–3) suggest that better performance can be expected from K^+ based electrolytes than their Li^+based counterparts. From the anion side, $TFSi^-$ outperforms the other studied ions. As for the medium, running the experiments in air or in the native electrolyte of the films is notably better than switching the medium to seawater or 1 M DPBS solution, which is most likely caused be the diffusion of foreign ions into the PPy film from the latter two. The overall best results were obtained with KTFSi electrolyte filled PPy films in air. According to our results (Table 1–3), our PPy films were performed better in air and their corresponding electrolyte solutions. Considering the actuation voltage, the tip displacements and applied voltages for samples dipped in Adriatic sea water and 1 M DPBS solution, could be due to possible ion exchange between the PPy films and the solution. The process of ion exchange is a well-known phenomena especially in the field of water treatment. Applying an external electric field will cause the electrotransport of sea water or the DPBS solution into the substrate layers. In the case of seawater mainly sodium and chloride ions will be incorporated into the films' porous structure [47]. The disadvantage of these PPy films, that they need to be constantly soaked and stored in their native electrolyte solution to prevent dehydration [41].

5. Conclusions

The objective of this study was to study the effects of different ionic electrolytes on the electroactuation behavior of polypyrrole films electrodeposited onto gilded PVDF membranes. Electrolytes composed of various dopant anions ($TFSi^-$, ClO_4^-, NO_3^-) and cations (K^+, Li^+) were tested in four different media: air, native electrolyte solution, Adriatic seawater and 1 M DPBS solution. Relevant quantitative electroactuation descriptors as peak voltage, peak half cycle duration, number of elecroactuation cycles, and days of electroactivity were determined experimentally. Potassium based electrolytes were found to improve the actuation mechanism in general. PPy films intercalated with KTFSi exhibited particulary good performance in air, remaining electroactive for over 40 days and whitstanding over 230 actuation cycles while maintaining at least 50% of their original displacement capacity. Considering our results, the electroactuator research could take advantage of the application of potassium salts as electrolytes in the electrosynthesis of polymer actuators and may open a feasible alternative in e.g. sustainable microelectric detection and artificial muscle systems development.

Declaration of Competing Interest

The authors declare that they have no known competing financial interests or personal relationships that could have appeared to influence the work reported in this paper.

CRediT authorship contribution statement

Zoltán Novák: Investigation, Writing – original draft, Writing – review & editing. **Gábor Kozma:** Investigation. **Ákos Kukovecz:** Supervision, Funding acquisition, Writing – review & editing.

Acknowledgment

The authors remember fondly the inspiring and cheerful personality of Professor István Pálinkó, an excellent mentor and very good friend. He is dearly missed. Project no. TKP2021-NVA-19 has been implemented with the support provided by the Ministry of Innovation and Technology of Hungary from the National Research, Development and Innovation Fund, financed under the TKP2021-NVA funding scheme.

Supplementary materials

Supplementary material associated with this article can be found, in the online version, at doi:10.1016/j.molstruc.2022.133057.

References

[1] A. Fannir, R. Temmer, G.T.M. Nguyen, L. Cadiergues, E. Laurent, J.D.W. Madden, F. Vidal, C. Plesse, Linear artificial muscle based on ionic electroactive polymer: a rational design for open-air and vacuum actuation, Adv. Mater. Technol. 4 (2019) 1800519, doi:10.1002/ADMT.201800519.
[2] J.M. McCracken, B.R. Donovan, T.J. White, Materials as Machines, Adv. Mater. 32 (2020) 1–48, doi:10.1002/adma.201906564.
[3] L. Chang, Y. Liu, Q. Yang, L. Yu, J. Liu, Z. Zhu, P. Lu, Y. Wu, Y. Hu, Ionic electroactive polymers used in bionic robots: a review, J. Bionic Eng. 155 (15) (2018) 765–782 2018, doi:10.1007/S42235-018-0065-1.
[4] S. Mun, S. Yun, S. Nam, S.K. Park, S. Park, B.J. Park, J.M. Lim, K.U. Kyung, Electroactive polymer based soft tactile interface for wearable devices, IEEE Trans. Haptics 11 (2018) 15–21, doi:10.1109/TOH.2018.2805901.
[5] V.F. Cardoso, D.M. Correia, C. Ribeiro, M.M. Fernandes, S. Lanceros-Méndez, Fluorinated polymers as smart materials for advanced biomedical applications, Polym. 10 (2018) 161 10 (2018) 161, doi:10.3390/POLYM10020161.
[6] M. Li, J. Chen, M. Shi, H. Zhang, P.X. Ma, B. Guo, Electroactive anti-oxidant polyurethane elastomers with shape memory property as non-adherent wound dressing to enhance wound healing, Chem. Eng. J. 375 (2019) 121999, doi:10.1016/J.CEJ.2019.121999.
[7] H. Palza, P.A. Zapata, C. Angulo-Pineda, H. P, P.A. Z, A.P. C, Electroactive smart polymers for biomedical applications, Materials 12 (2019) (Basel), doi:10.3390/ma12020277.
[8] M. Bharti, A. Singh, S. Samanta, D.K. Aswal, Conductive polymers for thermoelectric power generation, Prog. Mater. Sci. 93 (2018) 270–310, doi:10.1016/j.pmatsci.2017.09.004.
[9] M. Yellappa, J.S. Sravan, O. Sarkar, Y.V.R. Reddy, S.V. Mohan, Modified conductive polyaniline-carbon nanotube composite electrodes for bioelectricity generation and waste remediation, Bioresour. Technol. 284 (2019) 148–154, doi:10.1016/J.BIORTECH.2019.03.085.
[10] Z. Wang, J. Chen, Y. Cong, H. Zhang, T. Xu, L. Nie, J. Fu, Ultrastretchable strain sensors and arrays with high sensitivity and linearity based on super tough conductive hydrogels, Chem. Mater. 30 (2018) 8062–8069, doi:10.1021/ACS.CHEMMATER.8B03999.
[11] M.H. Naveen, N.G. Gurudatt, Y.B. Shim, Applications of conducting polymer composites to electrochemical sensors: a review, Appl. Mater. Today 9 (2017) 419–433, doi:10.1016/J.APMT.2017.09.001.
[12] A.P. Mártire, G.M. Segovia, O. Azzaroni, M. Rafti, W. Marmisollé, Layer-by-layer integration of conducting polymers and metal organic frameworks onto electrode surfaces: enhancement of the oxygen reduction reaction through electrocatalytic nanoarchitectonics, Mol. Syst. Des. Eng. 4 (2019) 893–900, doi:10.1039/C9ME00007K.
[13] S. Chandra, A. Dhawangale, S. Mukherji, Hand-held optical sensor using denatured antibody coated electro-active polymer for ultra-trace detection of copper in blood serum and environmental samples, Biosens. Bioelectron. 110 (2018) 38–43, doi:10.1016/J.BIOS.2018.03.040.
[14] I. Pugazhenthi, S.M. Safiullah, K.A. Basha, Photostable electroactive polymer based nanocomposite films for the protection of mild steel from corrosion, Polymers and Polymer, Composites 29 (2021) S130–S142, doi:10.1177/0967391120986506.
[15] Y. Yang, C. Feng, Y. Zhou, X. Zha, R. Bao, K. Ke, M. Yang, C. Tan, W. Yang, Achieving improved electromagnetic interference shielding performance and balanced mechanical properties in polyketone nanocomposites via a composite MWCNTs carrier, Compos. Part A Appl. Sci. Manuf. 136 (2020) 105967, doi:10.1016/J.COMPOSITESA.2020.105967.
[16] X. Wang, S.K. Mitchell, E.H. Rumley, P. Rothemund, C. Keplinger, High-strain peano-HASEL actuators, Adv. Funct. Mater. 30 (2020) 1908821, doi:10.1002/ADFM.201908821.
[17] U. Gupta, L. Qin, Y. Wang, H. Godaba, J. Zhu, Soft robots based on dielectric elastomer actuators: a review, Smart Mater. Struct. 28 (2019), doi:10.1088/1361-665X/ab3a77.
[18] K. Kaneto, F. Hata, S. Uto, Structure and size of ions electrochemically doped in conducting polymer, J. Micromech. Microeng. 28 (2018) 054003, doi:10.1088/1361-6439/aaaef5.
[19] R. Jain, N. Jadon, A. Pawaiya, Polypyrrole based next generation electrochemical sensors and biosensors: a review, TrAC Trends Anal. Chem. 97 (2017) 363–373, doi:10.1016/j.trac.2017.10.009.
[20] T.V. Vernitskaya, O.N. Efimov, Polypyrrole: a conducting polymer (synthesis, properties, and applications), Usp. Khim. 66 (1997) 502–505, doi:10.1070/rc1997v066n05abeh000261.
[21] O.I. Istakova, D.V. Konev, T.O. Medvedeva, E.V. Zolotukhina, M.A. Vorotyntsev, Efficiency of pyrrole electropolymerization under various conditions, Russ. J. Electrochem. 54 (2018) 1243–1251, doi:10.1134/S1023193518130190.
[22] F.C. Walsh, S. Wang, N. Zhou, The electrodeposition of composite coatings: diversity, applications and challenges, Curr. Opin. Electrochem. 20 (2020) 8–19, doi:10.1016/j.coelec.2020.01.011.
[23] M. Szabados, R. Mészáros, S. Erdei, Z. Kónya, Á. Kukovecz, P. Sipos, I. Pálinkó, Ultrasonically-enhanced mechanochemical synthesis of CaAl-layered double hydroxides intercalated by a variety of inorganic anions, Ultrason. Sonochem. 31 (2016) 409–416, doi:10.1016/J.ULTSONCH.2016.01.026.
[24] E. Markevich, G. Salitra, F. Chesneau, M. Schmidt, D. Aurbach, Very stable lithium metal stripping-plating at a high rate and high areal capacity in fluoroethylene carbonate-based organic electrolyte solution, ACS Energy Lett. 2 (2017) 1321–1326 10.1021/ACSENERGYLETT.7B00300/SUPPL_FILE/NZ7B00300_SI_001.PDF.
[25] Q. Wang, L. Jiang, Y. Yu, J. Sun, Progress of enhancing the safety of lithium ion battery from the electrolyte aspect, Nano Energy 55 (2019) 93–114, doi:10.1016/J.NANOEN.2018.10.035.
[26] W. Zhang, X. Chen, Y. Wang, L. Wu, Y. Hu, Experimental and modeling of conductivity for electrolyte solution systems, ACS Omega 5 (2020) 22465–22474, doi:10.1021/ACSOMEGA.0C03013.
[27] S. Sadki, P. Schottland, N. Brodie, G. Sabouraud, The mechanisms of pyrrole electropolymerization, Chem. Soc. Rev. 29 (2000) 283–293, doi:10.1039/a807124a.
[28] K. Kubota, M. Dahbi, T. Hosaka, S. Kumakura, S. Komaba, Towards K-ion and Na-ion batteries as "beyond Li-ion, Chem. Rec. 18 (2018) 459–479, doi:10.1002/tcr.201700057.
[29] H. Sun, P. Liang, G. Zhu, W.H. Hung, Y.Y. Li, H.C. Tai, C.L. Huang, J. Li, Y. Meng, M. Angell, C.A. Wang, H. Dai, A high-performance potassium metal battery using safe ionic liquid electrolyte, Proc. Natl. Acad. Sci. USA 117 (2020) 27847–27853, doi:10.1073/PNAS.2012716117/VIDEO-1.
[30] L. Fan, R. Ma, Q. Zhang, X. Jia, B. Lu, Graphite anode for a potassium-ion battery with unprecedented performance, Angew. Chem. Int. Ed. 58 (2019) 10500–10505, doi:10.1002/ANIE.201904258.
[31] J. Xie, J. Li, W. Zhuo, W. Mai, Recent progress of electrode materials cooperated with potassium bis(fluorosulfonyl)imide–containing electrolyte for K-ion batteries, Mater. Today Adv. 6 (2020) 100035, doi:10.1016/J.MTADV.2019.100035.
[32] B. Ji, F. Zhang, X. Song, Y. Tang, A novel potassium-ion-based dual-ion battery, Adv. Mater. 29 (2017) 1700519, doi:10.1002/adma.201700519.
[33] T. Yamamoto, R. Matsubara, T. Nohira, Highly conductive ionic liquid electrolytes for potassium-ion batteries, J. Chem. Eng. Data 66 (2021) 1081–1088, doi:10.1021/acs.jced.0c00879.
[34] S. Hara, T. Zama, W. Takashima, K. Kaneto, TFSI-doped polypyrrole actuator with 26% strain, J. Mater. Chem. 14 (2004) 1516–1517, doi:10.1039/b404232h.
[35] N. Nakamura, T. Yokoshima, H. Nara, T. Momma, T. Osaka, Suppression of polysulfide dissolution by polypyrrole modification of sulfur-based as in lithium secondary batteries, J. Power Sources 274 (2015) 1263–1266, doi:10.1016/J.JPOWSOUR.2014.10.192.
[36] T. Kadoyama, J. Yamasaki, F. Tsumuji, S. Takamiya, S. Ogihara, D. Hoshino, Y. Nishioka, Behaviors of polypyrrole soft actuators in LiTFSI or NaCl electrolyte solutions containing methanol, J. Mater. Sci. Chem. Eng. 01 (2013) 1–7, doi:10.4236/MSCE.2013.14001.
[37] M. Harjo, Z. Zondaka, K. Leemets, M. Järvekülg, T. Tamm, R. Kiefer, Polypyrrole-coated fiber-scaffolds: concurrent linear actuation and sensing, J. Appl. Polym. Sci. 137 (2020) 48533, doi:10.1002/APP.48533.
[38] S. Liu, N. Masurkar, S. Varma, I. Avrutsky, L.M. Reddy Arava, Experimental studies and numerical simulation of polypyrrole trilayer actuators, ACS Omega 4 (2019) 6436–6442, doi:10.1021/acsomega.9b00032.
[39] L.M. Duc, V.Q. Trung, Layers of inhibitor anion – doped polypyrrole for corrosion protection of mild steel, Mater. Sci. Adv. Top. (2013), doi:10.5772/54573.
[40] Q.-.G. Zhang, S.-.S. Sun, S. Pitula, Q.-.S. Liu, U. Welz-Biermann, J.-.J. Zhang, Electrical Conductivity of Solutions of Ionic Liquids with Methanol, Ethanol, Acetonitrile, and Propylene Carbonate, J. Chem. Eng. Data. 56 (2011) 4659–4664, doi:10.1021/je200616t.
[41] N. Masurkar, K. Jamil, L.M.R. Arava, Environmental effects on the polypyrrole tri-layer actuator, Actuators 6 (2017) 17 6 (2017) 17, doi:10.3390/ACT6020017.
[42] Q. He, Z. Liu, G. Yin, Y. Yue, M. Yu, H. Li, K. Ji, X. Xu, Z. Dai, M. Chen, The highly stable air-operating ionic polymer metal composite actuator with consecutive channels and its potential application in soft gripper, Smart Mater. Struct. 29 (2020), doi:10.1088/1361-665X/ab73e3.
[43] S. Amara, J. Toulc'Hoat, L. Timperman, A. Biller, H. Galiano, C. Marcel, M. Ledigabel, M. Anouti, Comparative study of alkali-cation-based (Li +, Na +, K +) electrolytes in acetonitrile and alkylcarbonates, ChemPhysChem 20 (2019) 581–594, doi:10.1002/cphc.201801064.

[44] T.G. Noh, Y. Tak, J. Do Nam, H. Choi, Electrochemical characterization of polymer actuator with large interfacial area, Electrochim. Acta 47 (2002) 2341–2346, doi:10.1016/S0013-4686(02)00089-0.
[45] M. Zhou, P. Bai, X. Ji, J. Yang, C. Wang, Y. Xu, Electrolytes and interphases in potassium ion batteries, Adv. Mater. 33 (2021) 1–22, doi:10.1002/adma.202003741.
[46] J.J. Hu, G.K. Long, S. Liu, G.R. Li, X.P. Gao, A LiFSI–LiTFSI binary-salt electrolyte to achieve high capacity and cycle stability for a Li-S battery, Chem. Commun. 50 (2014) 14647–14650, doi:10.1039/C4CC06666A.
[47] N.P. Berezina, N.A. Kononenko, O.A. Dyomina, N.P. Gnusin, Characterization of ion-exchange membrane materials: properties vs structure, Adv. Colloid Interface Sci. 139 (2008) 3–28, doi:10.1016/J.CIS.2008.01.002.